Journal of Molecular Liquids 275 (2019) 290–296

Contents lists available at ScienceDirect

Journal of Molecular Liquids

journal homepage: www.elsevier.com/locate/molliq

Surface behavior of low-temperature molten salt mixtures during the transition from liquid to solid

Radha G. Bhuin [a,*], Patrick Schreiber [a], Bettina S.J. Heller [a], Marlene Scheuermeyer [b], Peter Wasserscheid [b,c], Hans-Peter Steinrück [a], Florian Maier [a,*]

[a] Lehrstuhl für Physikalische Chemie 2, Friedrich-Alexander-Universität Erlangen-Nürnberg, Egerlandstr. 3, 91058 Erlangen, Germany
[b] Lehrstuhl für Chemische Reaktionstechnik, Friedrich-Alexander-Universität Erlangen-Nürnberg, Egerlandstr. 3, 91058 Erlangen, Germany
[c] Forschungszentrum Jülich, Helmholtz-Institut Erlangen-Nürnberg für Erneuerbare Energien (IEK 11), Egerlandstr. 3, 91058 Erlangen, Germany

ARTICLE INFO

Article history:
Received 7 November 2018
Accepted 14 November 2018
Available online 15 November 2018

Keywords:
Ionic liquids
Molten salts
Angle-resolved X-ray photoelectron spectroscopy

ABSTRACT

We report on surface investigations of cesium and tetraphenylphosphonium bis(trifluoromethylsulfonyl)imide ($Cs[Tf_2N]$, $[PPh_4][Tf_2N]$) molten salts and their mixtures. Depending on composition, these ionic compounds combine low melting points with exceptionally high thermal stability, and thus, exhibit considerably enlarged thermal operation windows compared to conventional ionic liquids. To elucidate their liquid-solid transition behavior in the near-surface region, temperature-dependent angle-resolved X-ray photoelectron spectroscopy (ARXPS) investigations were performed using our unique laboratory electron spectrometer DASSA ("Dual Analyzer System for Surface Analysis"), dedicated for investigations of macroscopic liquid samples. We followed temperature-induced changes in bulk and surface composition within the first nanometers of the neat salt melts and of $Cs[Tf_2N] : [PPh_4][Tf_2N] = 3 : 1$ and $1 : 3$ mixtures. In the mixtures, pronounced surface enrichment of Cs^+ on expense of the bulky $[PPh_4]^+$ ions was found in the liquid state at temperatures close to the liquid-solid transition. In the solid state of $Cs[Tf_2N]$-rich mixtures, $[PPh_4]^+$ completely vanishes from the near-surface region probed by XPS.

1. Introduction

Starting in the late nineties, research on ionic liquids (ILs) has received profound and increased scientific attention. ILs are a new class of materials composed solely of cations and anions with low melting temperatures, typically well below 100 °C. They provide outstanding physicochemical properties with respect to vapor pressure, charge density, polarity, viscosity, heat capacity, coordination behavior, and ion conductivity, to name a few. Due to their structural diversity, these properties can be tuned in a wide range combining suitable cations and anions [1–6]. This empowers ILs to be potentially used in various applications including supercapacitors and batteries, fuel and solar cell, electrochemistry, semiconductors, nanotechnology, catalysis, green chemistry, green engineering, and many others [2,4–7]. Most of these applications require a detailed understanding of the surface and interface properties of ILs. Due to their extremely low vapor pressure, as compared to conventional liquids such as water, alcohol, *etc.*, ILs provide the unique opportunity to investigate them under a fully controlled environment using sophisticated surface analytical techniques in ultra-high vacuum (UHV). Starting around 2005, an increasing number of surface analytical techniques has been successfully employed to examine surface phenomena of ILs, such as surface segregation/termination/enrichment effects, re-orientation of ions at the outermost surfaces, surface reactions, and many more [8–19]. The roles of liquid-vacuum and liquid-solid interfaces become particularly important in the context of high surface area systems, which are relevant for applications of ILs in catalysis. In this context, several novel catalyst concepts have been introduced, *e.g.* the "Supported Ionic Liquid Phase (SILP)" [20,21] and the "Solid Catalyst with Ionic Liquid Layer (SCILL)" [21,22] approaches. In both, an extremely thin IL film covers a porous support. In course of biphasic reactions, reactants enter and products leave the liquid film through its surface. Thereby, the outermost layers become a prominent part of the whole system. Preferential surface enrichment and depletion effects, which lead to deviations of the surface composition from the bulk composition, will have an impact on the performance of these high-surface area systems, *e.g.* by influencing the overall kinetics of the reaction.

Despite their successful application in various catalytic processes, most ILs containing organic ions are limited by their stability. For typical ILs, reactions under real conditions should be carried out well below 250 °C to avoid substantial evaporation and decomposition losses [23]. In catalysis, increasing reaction rates by raising the reaction temperature is particularly advantageous when less expensive catalysts, which often

* Corresponding authors.
E-mail addresses: radha.g.bhuin@fau.de (R.G. Bhuin), florian.maier@fau.de (F. Maier).

https://doi.org/10.1016/j.molliq.2018.11.056

are less active, are used to replace high-cost catalysts, *e.g.* nickel instead of platinum for hydrogenation reactions. Replacing conventional IL cations and anions by inorganic ions such as metal ions leads to an increase in thermal stability, but also to higher melting points [24]. The latter disadvantage can be partially compensated by mixing different ionic compounds, in order to form eutectic systems with low melting points and thus, a large liquid phase window. Recently, we reported the first study on high-temperature-stable/low-melting salt mixtures of cesium bis(trifluoromethylsulfonyl)imide and tetraphenylphosphonium bis (trifluoromethylsulfonyl)imide ($Cs[Tf_2N]$ and $[PPh_4][Tf_2N]$). Close to the eutectic molar composition of $Cs[Tf_2N] : [PPh_4][Tf_2N] = 2.13 : 1$ (68 mol% $Cs[Tf_2N]$), these mixtures exhibit melting points below 100 °C [24]. The melting diagram of the two salts, which are immiscible in the solid state, is shown in Fig. 1, as derived from differential scanning calorimetry (DSC) [24]. Notably, pronounced supercooling effects and even the absence of crystallization were observed in DSC while cooling, particularly for Cs^+-lean mixtures. Therefore, the phase transition temperatures shown in Fig. 1 are solely derived during heating. In the course of a general characterization of these mixtures by angle-resolved X-ray photoelectron spectroscopy (ARXPS), we already reported a preferential surface depletion of the $[PPh_4]^+$ cation at 130 °C in the liquid state for a $Cs[Tf_2N] : [PPh_4][Tf_2N] = 3 : 1$ mixture (75 mol% $Cs[Tf_2N]$) [24].

Herein, we now focus on the near-surface region of two $Cs[Tf_2N]$/$[PPh_4][Tf_2N]$ mixtures at different temperatures in order to systematically study these surface effects, particularly in the context of liquid-solid phase transitions. The results are obtained for a Cs^+-rich 3 : 1 (75 mol% $Cs[Tf_2N]$) and for a Cs^+-lean 1 : 3 (25 mol% $Cs[Tf_2N]$) mixture, that is, at both sides of the eutectic composition of 68 mol% $Cs[Tf_2N]$. Upon heating under thermodynamic equilibrium conditions, we expect from the bulk phase diagram that the 3:1 mixture (left dotted line in Fig. 1) starts to melt at around 96 °C. It forms an eutectic melt with 68 mol% $Cs[Tf_2N]$ in the liquid state, together with solid $Cs[Tf_2N]$ crystals, which disappear at around 104 °C, when a homogeneous melt with 3 : 1 composition is reached. The 1 : 3 mixture (right dotted line in Fig. 1) also starts to melt at 96 °C, forming the eutectic melt together with solid $[PPh_4][Tf_2N]$ crystals, until at 113 °C, a homogeneous melt with 1 : 3 composition is reached. In this work, we will show that during solidification of the Cs^+-rich 3 : 1 mixture upon cooling, the $[PPh_4]^+$ cations completely leave the near-surface region of ~9 nm probed by ARXPS. We also observe a strong supercooling effect accompanied by depletion of $[PPh_4]^+$ cations in the Cs^+-lean 1 : 3 mixture until room temperature. Both the mixtures almost regain their initial composition in the near-surface region upon heating back to their starting point to the liquid phase. As far as we are aware, this is the first systematic liquid-solid phase transition investigation for purely ionic systems using XPS under well-controlled ultra-high vacuum (UHV) conditions.

2. Experimental section

2.1. Materials

$[PPh_4][Tf_2N]$ and $Cs[Tf_2N]$ were synthesized in our laboratories. The detailed procedure of the synthesis was given elsewhere [24]. The mixtures of $Cs[Tf_2N]$ and $[PPh_4][Tf_2N]$ were prepared by mixing the powders of the single components in the desired molar ratios, followed by subsequent melting. The latter step was performed while stirring the melt over more than one hour under vacuum (pressure ~0.5 mbar) to ensure homogeneous mixing and drying. After cooling, dry powders were obtained with white color.

2.2. Differential scanning calorimetry (DSC) measurements

For the phase diagram and melting point measurements, heating and cooling cycles were carried out using a dynamic DSC setup Phoenix DSC 204 F1 (Netzsch). 10 mg of each mixture was weighted in aluminum crucibles. The heating and cooling rates were 2 K min^{-1}. The transition temperatures were determined from the heating curves to avoid supercooling effects (see also Results and Discussion).

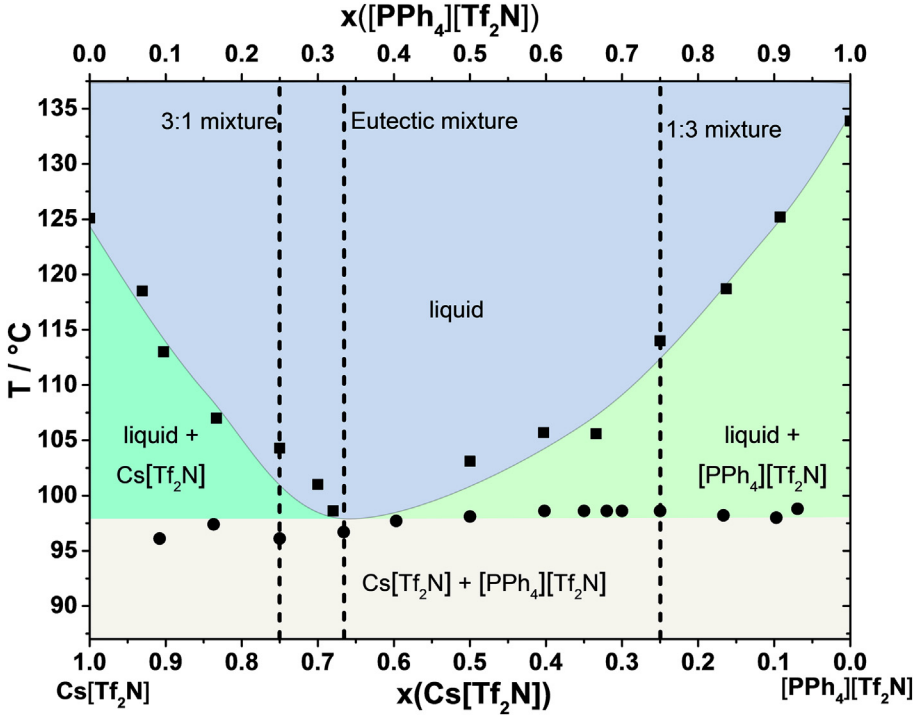

Fig. 1. Melting phase diagram of $Cs[Tf_2N]$ and $[PPh_4][Tf_2N]$ mixtures, adapted from Ref. [24]. Dotted lines indicate the two mixtures under investigation and the eutectic composition with melting point minimum.

2.3. ARXPS measurements

The surface studies were performed using our new and unique laboratory electron spectrometer DASSA ("Dual Analyzer System for Surface Analysis"), dedicated to investigations of liquid samples. The details of the spectrometer are given elsewhere [25]. In short, it comprises an UHV chamber equipped with two electron analyzers (ARGUS, Omicron), for simultaneous measurements of a horizontally mounted liquid sample at emission angles of 0° and 80°, relative to the surface normal. Measurements at 0° are considered as bulk sensitive (information depth 7–9 nm), and measurements at 80° as surface sensitive (information depth 1–1.5 nm). In contrast to conventional ARXPS using one analyzer and rotating the sample for subsequent normal and grazing emission measurements, simultaneous measurements at 0° and 80° provide the advantage of reduced measurement time and minimized radiation exposure. Moreover and even more important for studies with supercooled liquids is the fact that the risk of different phases being present in subsequent 0° and 80° measurements (*e.g.* due to spontaneous crystallization) is completely avoided with our new setup. Monochromated Al K_α radiation ($h\nu = 1486.6$ eV, anode voltage = 14 kV, $I = 10$ mA; spot size of 1.0 mm × 2.0 mm at sample) was used to irradiate the sample at the magic angle of 54.7° with respect to both analyzers. XP spectra of the various core levels were recorded with a pass energy of 35 eV, resulting in a combined energy resolution of ~0.4 eV; 200 eV were used for survey spectra. The spectra are presented as obtained from the instrument without any charge correction. To compensate for their lower intensity, the 80° spectra are re-scaled by a common geometry factor as previously reported [25].

The mixtures were introduced into the UHV system as powders and heated to above their melting point *in situ* prior to measuring. In order to achieve identical film thicknesses, we always completely filled the reservoirs of the sample holder (~0.5 mm in depth). All samples were weighted *ex-situ* before and after measurements. Molten samples were ready to be measured when a base pressure of about 10^{-7} mbar was reached in the fast-entry loadlock (FEL), typically after keeping the sample overnight in the FEL. All temperature-dependent experiments started at high temperatures with the entire samples in the liquid state. This approach was chosen, because all core level signals remained unchanged with time in this state while for solid samples at room temperature irreversible beam damage effects in terms of additional fluoride signals (not shown) were observed due to decomposition of $[Tf_2N]^-$ after prolonged X-ray exposure. In order to further minimize beam damage, samples were only exposed to X-rays once the desired temperatures were reached and not in-between. Note that X-ray beam damage effects during XPS on solid ionic samples were reported in the past [26]. Sample temperatures were measured using a type K thermocouple directly attached to the sample holder, with an absolute accuracy of about ±5 °C, and a reproducibility and stability of ±1 °C.

The XP spectra were analyzed using the CasaXPS software (version 2.3.16). Wherever surface stoichiometry was calculated, peaks were fitted; otherwise, numeric integration was sufficient to derive relative intensity changes. For peak fitting, we used a Gaussian-Lorentzian profile with 30% Lorentz contribution, and the area ratios and peak separation for spin-orbit-coupled states were constrained.

3. Results and discussion

The ARXPS measurements for pure Cs[Tf_2N], pure [PPh_4][Tf_2N], and for mixtures at both sides of the eutectic composition, that is, for Cs[Tf_2N] : [PPh_4][Tf_2N] = 3 : 1 (="Cs^+-rich") and for Cs[Tf_2N] : [PPh_4][Tf_2N] = 1 : 3 (="Cs^+-lean"), were performed during cooling from a temperature, where the sample was completely molten. As detailed in the Experimental Section, irreversible beam damage effects were observed after prolonged X-ray exposure for solid samples at room temperature. Once a targeted temperature was reached, the temperature was held constant during ARXPS. As we will discuss in the following, pronounced supercooling effects well below the melting temperatures (as given by the phase diagram shown in Fig. 1) were observed, particularly for the neat [PPh_4][Tf_2N] salt and for the Cs^+-lean system. Since solidification for supercooled systems is a kinetic effect, slightly different onset temperatures for solidification were observed in repeated experiments using samples with identical composition. Hence, the spectral series shown here were selected as representative cases to discuss the main phenomena observed.

3.1. Temperature-dependent ARXPS of pure Cs[Tf_2N] and [PPh_4][Tf_2N]

We first present XP spectra collected during cooling of the neat compounds Cs[Tf_2N] and [PPh_4][Tf_2N] from the liquid to the solid state; see Fig. 2. As it will be detailed below, both salts show supercooling behavior (see DSC curves in Fig. S4 in SI), that is, they remain liquid until well below their melting points of 125 °C for Cs[Tf_2N] and 134 °C for [PPh_4][Tf_2N]. These melting points (see also Fig. 1) are derived from the DSC curves during heating [24].

Both neat molten salts were first characterized in the liquid phase at high temperature. For Cs[Tf_2N], the survey 0° and 80° ARXP spectra at 145 °C display the presence of all elements, namely Cs, F, O, N, C, and S at their expected binding energies (see Fig. S1 in SI, left panel). The absence of a Si signal, which is an indication for a common surface-active polysiloxane contamination [27], confirms the high purity of the sample. The stoichiometry derived from the bulk-sensitive 0° spectra (Table S1 in SI) shows small deviations, which for some elements are a little larger than our typical experimental error of ±15%. Since the results for the mixtures are mainly derived from the Cs $3d_{5/2}$ and the C 1s core levels, these deviations do not play a significant role in the following.

Temperature-dependent ARXP spectra for Cs[Tf_2N] upon cooling from 145 to 100 °C are presented in the left panel of Fig. 2, where the Cs $3d_{5/2}$ and C 1s regions are shown. The Cs $3d_{5/2}$ peak at ~725 eV is representative of the cation, and the C 1s peak at ~293 eV of the anion. The corresponding F 1s, O 1s, and S 2p signals are shown in Fig. S2 of SI. The dotted vertical lines indicate the peak positions at 145 °C. Upon cooling, at 130 °C and at 115 °C no pronounced changes are seen. At 100 °C, both the cation and anion peaks are slightly broadened and significantly shifted to higher binding energies by about 1.4 eV. As has been discussed for other systems, such shifts are a clear indication of solidification in ILs resulting in sample charging [25]. Compared to the melting point of 125 °C of Cs[Tf_2N], the onset of charging was found to be shifted by about 25 °C to lower temperatures due to supercooling. The overall similar signal intensities at 0° (black) and 80° (red) indicate that cations and anions are more or less homogeneously distributed within the outermost surface layers probed in 80° compared to the average composition probed in 0°. Nevertheless, for all temperatures, and most pronounced for the lowest temperature of 100 °C, a slightly smaller Cs signal is seen in the surface-sensitive 80° geometry as compared to the 0° spectra in Fig. 2 (left); the same is true for the O 1s ARXP spectra. In contrast, the F 1s intensity originating from the CF_3-groups is larger in 80° (see Fig. S2 in SI). Our ARXPS data thus clearly indicate that in the outermost surface layer, the anions are preferentially oriented in a cis-configuration with the non-polar CF_3-groups pointing towards the vacuum side and the SO_2-groups pointing towards the bulk, coordinating the Cs^+ cations.

For neat [PPh_4][Tf_2N], the survey spectra in the liquid phase again reveal all expected elements, that is, F, O, N, C, S, and P at their expected binding energies (Fig. S1 in SI, right panel). In addition, small Si 2s and 2p signals are seen at ~153 and ~103 eV, respectively, indicating a minor polysiloxane contamination. The fact that these signals are only observed at 80° indicates that the polysiloxane is enriched at the outermost surface. The mean stoichiometry derived from the spectra at 0° (Table S2 in SI) shows a very good agreement with the nominal compositions.

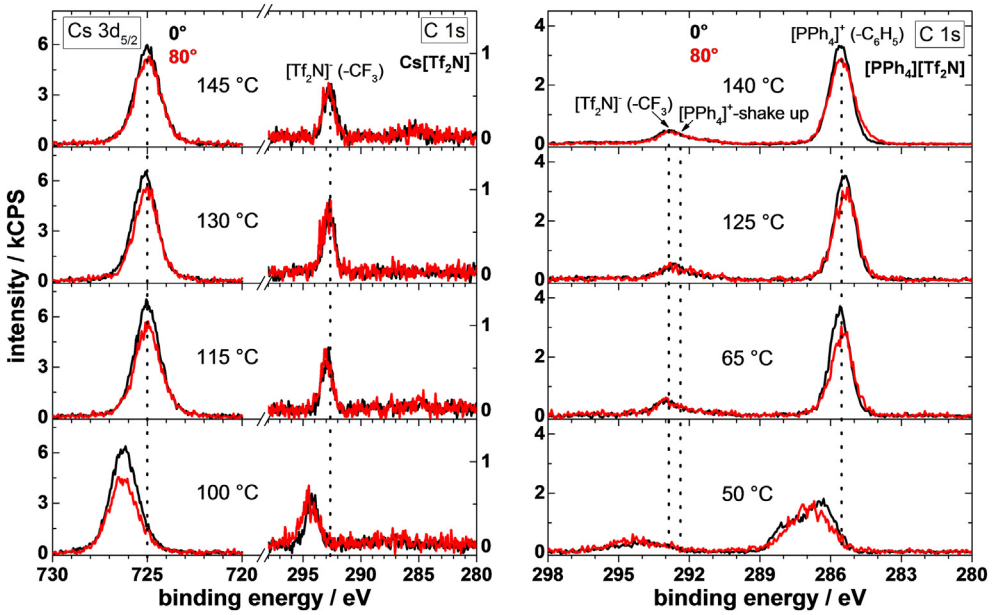

Fig. 2. ARXP spectra taken at 0° (bulk sensitive, black) and 80° (surface sensitive, red) electron emission angle for pure Cs[Tf_2N] in the Cs $3d_{5/2}$ and C 1s region (left panel), and for pure [PPh_4][Tf_2N] in the C 1s region (right panel during cooling).

The right panel in Fig. 2 displays the temperature-dependent ARXP spectra for [PPh_4][Tf_2N] in the C 1s region. The peak at ~293 eV is representative of the CF_3-group of the anion, and the peak at ~285.5 eV stems from the phenyl rings of the cation; note that due to the small cross-section of the P 2p core level, we have chosen the phenyl C 1s signal to represent the cation. Due to the π-electron-systems of the phenyl rings, we also find a broad shake-up feature centered at ~292.4 eV (indicated by an arrow in Fig. 2), which overlaps with the C 1s signal of the CF_3 groups. To unambiguously determine the binding energy and relative intensity of this shake-up signal, we also measured the C 1s spectrum of [PPh_4]Cl, which does not possess CF_3 groups (Fig. S3 in SI). For this salt, the shake-up signal is measured as isolated peak, separated by 6.8 eV from the phenyl C 1s peak, with ~10% of its intensity (Fig. S3 in SI). We have used these fitting parameters to obtain correct values for the quantitative composition analysis of the [PPh_4][Tf_2N]-containing systems with respect to the number of phenyl carbon atoms.

From the very similar signal intensities of $[PPh_4]^+$ cations and $[Tf_2N]^-$ anions at 0° and 80°, we conclude that between 140 and 65 °C both ions are homogeneously distributed within the analyzed volume ruling out pronounced orientation effects in the outermost surface layer. Upon further cooling, we observe changes at 50 °C, where both cation and anion peaks are broader and shifted to higher binding energy by more than 1 eV. Notably, this temperature is about 80 °C below the melting point. A similar broadening and uniform peak shift at 50 °C is seen also for the other anion core levels (see Fig. S2 in SI). As already pointed out above, the broadening and shifting of XPS peaks to higher binding energy indicates a charging of the sample, which typically is only observed for solid IL samples [8,25]. The larger freezing delay of ~80 °C for [PPh_4][Tf_2N] compared to ~25 °C for Cs[Tf_2N] demonstrates that, despite their very similar melting temperatures, supercooling apparently is more pronounced for [PPh_4][Tf_2N]. This finding was also confirmed by DSC, where the solidification temperatures during cooling are found to be significantly lowered by several tens of °C for the phosphonium salt (see also two representative DSC cycles for Cs[Tf_2N] and [PPh_4][Tf_2N] in Fig. S4, SI). Notably, a large scatter of the solidification temperatures was observed in several DSC heating/cooling cycles even for the same mixture samples, whereas during heating, the endothermic peaks indicating melting were reproducible within a few °C.

It is important to note again that no unexpected XPS signal changes were observed during all temperature-dependent experiments when starting with the liquid samples. Thus, both ILs can be assumed to be relatively stable under X-ray irradiation in vacuum even when solidification started, despite the fact that at room temperature and upon long-term exposure, decomposition effects in alkali $[Tf_2N]^-$ salts were found by us and by others [26].

3.2. Temperature-dependent ARXPS of the Cs^+-rich Cs[Tf_2N] : [PPh_4][Tf_2N] = 3 : 1 mixture

Fig. 3 displays the ARXP spectra of a 3 : 1 mixture of Cs[Tf_2N] and [PPh_4][Tf_2N], that is, $Cs_{0.75}[PPh_4]_{0.25}[Tf_2N]$ collected during cooling from 145 to 95 °C, followed by heating back to 145 °C. The left panel shows the Cs $3d_{5/2}$ peak of the Cs^+ cation at ~725 eV, and the C 1s peaks of the $[PPh_4]^+$ cation at 285.5 eV and the CF_3-groups of the $[Tf_2N]^-$ anion at ~293 eV. Additionally, the F 1s, O 1s, and S 2p peaks of the anion are displayed in the right panel of Fig. 3.

The XP spectra at 145 °C reveal sharp core level signals of all the elements with the expected intensities (±15%; see data for 0° in Table S3, SI) at the binding energies of the single liquid salts, which indicates that the mixture is liquid at this temperature, as is expected from the phase diagram (Fig. 1). The comparison of the spectra at the two emission angles shows very similar signals at 0° and 80°; only the phenyl C 1s signal at 285.5 eV (Fig. 3, left panel, topmost spectrum) is significantly smaller at 80°. This observation is in line with our earlier reports for the identical mixture composition measured at 130 °C [24]. The situation is even more pronounced at 110 °C, where the phenyl C 1s signal at 80° is ~40% smaller than at 0°, which indicates a pronounced depletion of the $[PPh_4]^+$ cation from the surface. The Cs^+ intensity does not show differences with emission angle, but its overall intensity has significantly increased.

Lowering the temperature by only 5 °C to 105 °C leads to a complete disappearance of the $[PPh_4]^+$ signal in 0° and 80°. This observation indicates that the bulky $[PPh_4]^+$ cations completely left the XPS information depth, and that the topmost of 7–9 nm thus, only consist of pure Cs[Tf_2N]. This conclusion is confirmed by the uniform increase in intensity of all other signals in 0° shown in Fig. 3, which results from the overall increase of the IL density, when replacing the large $[PPh_4]^+$ cation by the considerably smaller Cs^+ cation. In the liquid state at 200 °C, the molar volumes of neat [PPh_4][Tf_2N] and Cs[Tf_2N] are about 0.5 and 0.2 dm^3/mol, respectively, as derived from the measured mass densities

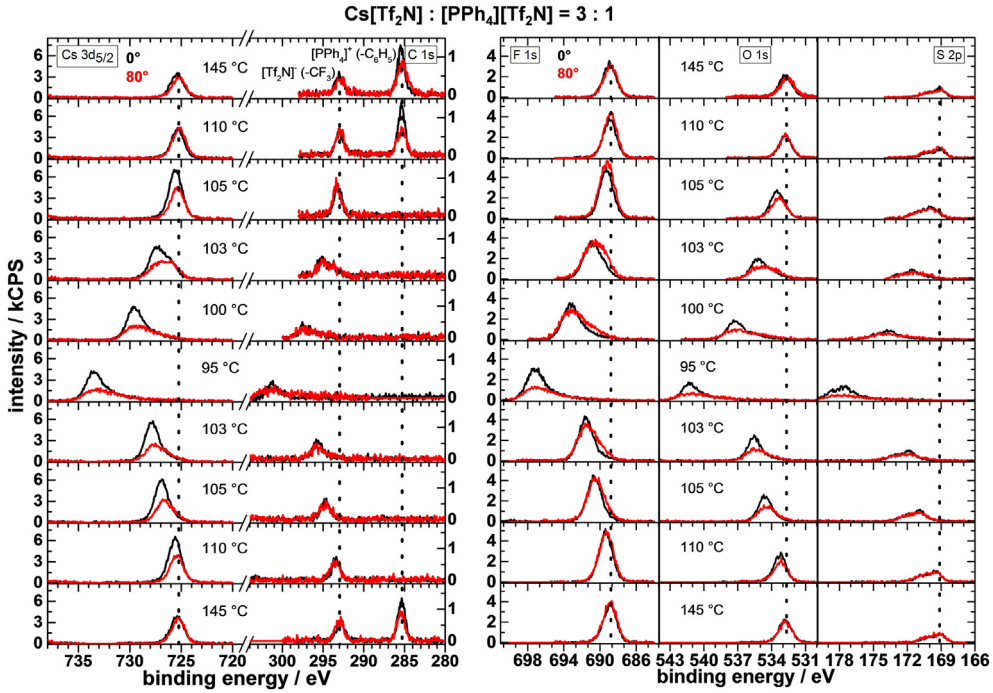

Fig. 3. ARXP spectra taken at 0° (bulk sensitive, black) and 80° (surface sensitive, red) electron emission angle for the 3 : 1 mixture of Cs[Tf_2N] : [PPh_4][Tf_2N] in the Cs $3d_{5/2}$ and C 1s region (left panel) and F 1s, O 1s, and S 2p region (right panel), during cooling (top half) and heating (bottom half).

[24]. Notably, the F 1s and C_{CF3} 1s signals at 80° increase compared to the 0° spectra, while the Cs $3d_{5/2}$ and the O 1s signals show the opposite trend. This behavior points at the same preferential orientation at the surface as discussed above for neat Cs[Tf_2N]: in the outermost surface layer, the $[Tf_2N]^-$ anion in cis-configuration is oriented such that the CF_3-groups are preferentially pointing towards the vacuum with the oxygen atoms coordinating the Cs^+ cation are pointing towards bulk. Moreover, the spectra at 105 °C are slightly broadened and slightly shifted to higher binding energy by 0.3–0.8 eV. The overall shifts to higher binding energies are assigned – as in the case of neat Cs[Tf_2N] at 100 °C (see Fig. 2) – to the onset of solidification accompanied by sample charging.

Upon further lowering the temperature by 2 °C, the signal broadening and shifting are even more pronounced. This spectral broadening accompanied by increasing overall shifts to higher binding energy continues until the lowest temperature of 95 °C in this series was reached. From 105 °C on, only Cs[Tf_2N] signals are detected in XPS, our results indicate a growing surface layer of solid Cs[Tf_2N], which displays more and more charging with increasing thickness; at 105 °C, this solid layer already must have exceeded 9 nm thickness, which is the maximum probing depth in 0° of our ARXPS setup. It is important to note that the XP spectra at 105 °C and lower temperatures thus do not provide any further information on composition changes beneath this layer, that is, inside the bulk, which might still become an eutectic melt with additional [PPh_4][Tf_2N] crystallization at around 96 °C according to the thermodynamic phase diagram, or, in case of supercooling might stay liquid. The onset of solid Cs[Tf_2N] formation at the surface occurs very close to the temperature expected from the phase diagram shown in Fig. 1. This rules out strong supercooling effects for the 3 : 1 mixture. Notably, in a separate experiment with a freshly prepared 3 : 1 mixture, the disappearance of $[PPh_4]^+$ started at around 100 °C (instead of 105 °C as found above), indicating some variation in temperature.

After reaching 95 °C, the sample was heated again to check for the reversibility of the process. The spectra obtained are displayed in the bottom half of Fig. 3: the XP peaks stepwise shift back with some small hysteresis effects, as seen by the 110 °C spectra, which are virtually identical to the 105 °C spectra during the cooling sequence. After the last heating step to 145 °C, the spectra of the mixture show the re-appearance of the $[PPh_4]^+$ cation and are virtually identical to the data of the 3 : 1 mixture at the starting point. Our observations indicate that the solid Cs[Tf_2N] layer melts again during heating and decreases in thickness, which goes along with reduced charging.

At the moment, the reason for the observed formation of a solid Cs[Tf_2N] surface is not clear yet. The preferential presence of Cs[Tf_2N] in the topmost surface layer of the mixture even in the liquid state was unambiguously observed by ARXPS. Since this behavior is most likely driven by minimizing surface free energy, this pre-ordering might facilitate later crystallization forming the solid surface layer.

3.3. Temperature-dependent ARXPS of the Cs^+-lean Cs[Tf_2N] : [PPh_4][Tf_2N] = 1 : 3 mixture

We conducted a similar experiment with a Cs^+-lean mixture of Cs[Tf_2N] and [PPh_4][Tf_2N] with a molar ratio of 1 : 3, that is, $Cs_{0.25}[PPh_4]_{0.75}[Tf_2N]$ (right side of the phase diagram of Fig. 1). The corresponding Cs $3d_{5/2}$, C 1s, and F 1s spectra are shown in Fig. 4. At 140 °C, where the mixture is fully liquid, the XP spectra reveal all core level signals at their expected binding energies and intensities (see composition Table S4 in SI). The nearly identical signals of all peaks at 0° and 80° indicate that the anion and both cations are both present at the surface layer and in the near-surface region probed by XPS, again with a minor surface depletion of the $[PPh_4]^+$ and enrichment of the Cs^+ cations. Lowering the temperature to 90 °C does not cause any significant changes in the spectra.

Upon cooling to 75 °C, noticeable changes are observed. The C 1s signal of the $[PPh_4]^+$ cation has significantly decreased in both emission angles, while the intensity of Cs $3d_{5/2}$ shows a pronounced increase. This observation indicates that the Cs^+ ion strongly is enriched and at the same time the $[PPh_4]^+$ ion is strongly depleted from the topmost 9 nm, that is, the information depth probed by XPS. Additional information can be derived from the F 1s signal. Its overall increase at 75 °C is attributed to the higher IL (and thus anion) density when the smaller Cs^+ cations are enriched in the surface-near region. The larger F 1s

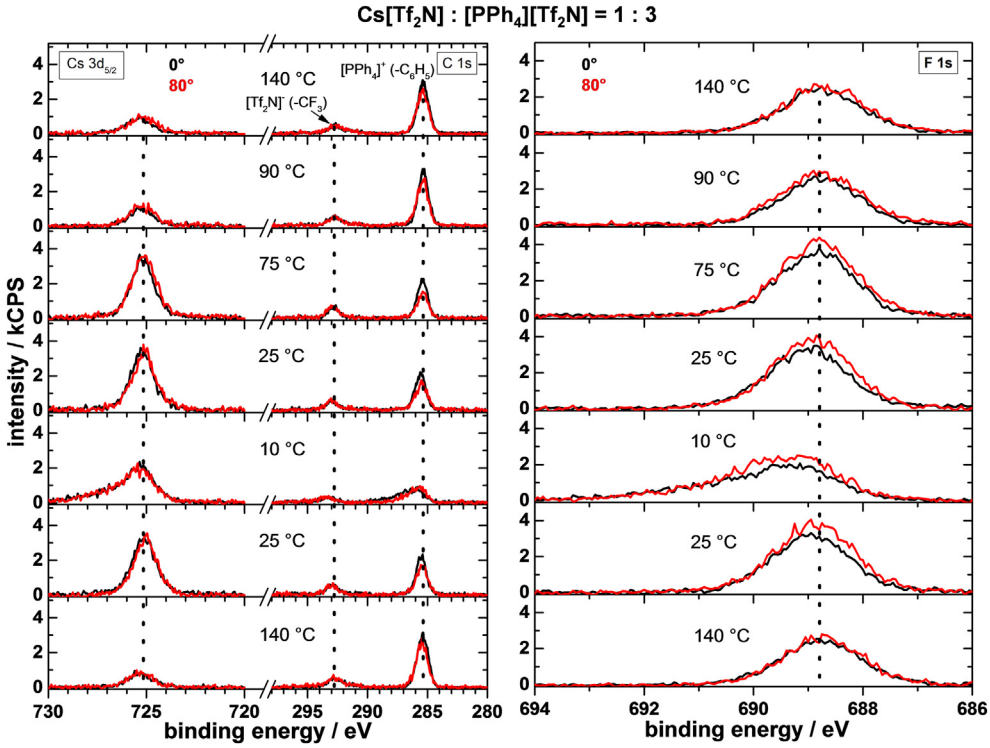

Fig. 4. ARXP spectra taken at 0° (bulk sensitive, black) and 80° (surface sensitive, red) electron emission angle for 1 : 3 mixture of $Cs[Tf_2N]$: $[PPh_4][Tf_2N]$ in the Cs $3d_{5/2}$ and C 1s region (left panel) and F 1s region (right panel) during cooling and heating.

signal at 80° as compared to 0° is attributed to the preferential orientation of the anion in cis-configuration with the CF_3-groups pointing towards the vacuum side, and the O atoms coordinating to the Cs^+ ion. Unlike the Cs^+-rich mixture discussed above, we do not observe any shifts or broadening of the peaks indicating charging effects until 25 °C. Moreover, the $[PPh_4]^+$ signal does not completely disappear between 75 and 25 °C; the Cs^+ : $[PPh_4]^+$ ratio as derived from the 0° Cs $3d_{5/2}$ and phenyl C 1s signal intensities in this temperature range is about 2 : 1 (=0.67), which is close to the eutectic composition (= 0.68). Hence, we propose that between 90 and 75 °C, solid $[PPh_4][Tf_2N]$ crystals are formed in the bulk, away from the near-surface region probed by XPS. Therefore, this region is depleted from $[PPh_4]^+$ until the eutectic melt composition was reached. Since no charging effects were observed down to 25 °C, we rule out complete solidification of our sample. Hence, ion mobility – that is expected to decrease with decreasing temperature – was apparently still high enough in this eutectic melt to compensate for the loss of negative charge through photoelectrons in XPS. This observation points to pronounced supercooling effects in this melt (most likely, an amorphous glassy state). Only when reaching the lowest temperature of 10 °C in our series, the spectra broadened and somewhat shifted to the higher binding energies, indicating sample charging due to a further reduction in ion mobility. Heating back to 25 °C restores the 25 °C-spectra of the cooling cycle showing full reversibility. Finally, we heated this mixture back to 140 °C. The spectra were found to be identical to the ones at the beginning of the cooling sequence indicating that the composition in the near-surface region could be fully recovered (see Fig. 4, first and last spectra set).

4. Summary and conclusions

We present the first ARXPS phase transition monitoring for the particular example of $Cs[Tf_2N]$/$[PPh_4][Tf_2N]$ molten salt mixtures with low melting points and high temperature stability. In two different mixtures at both sides of the eutectic composition, we demonstrate that $[PPh_4]^+$ ions are preferentially depleted from the surface when the mixtures are cooled down. In the surface layer, the $[Tf_2N]^-$ anion in cis-orientation is oriented such that the CF_3 groups preferentially are protruding towards vacuum; the SO_2-groups point towards the bulk and coordinate the Cs^+ cations, which are thus also away from the outermost surface. In the Cs^+-rich 3 : 1 mixture, solidification, as indicated by surface charging, starts from the surface inwards, and goes along with a $[PPh_4]^+$ depletion in the near-surface region probed by XPS to well below the detection limit of our measurement. To best of our knowledge, this is the first time surface freezing of molten salts with a change in surface composition is observed. For the Cs^+-lean 1 : 3 mixture, we observe the formation of an eutectic melt in the near-surface region between 90 and 75 °C, which is below the temperature of ~98 °C expected from the phase diagram. In this supercooled state, $[PPh_4]^+$ is significantly depleted and Cs^+ is enriched in the surface near region probed by XPS. Only at 10 °C, that is, well below room temperature, the near-surface region of the Cs^+-lean mixture shows indications for freezing.

We want to emphasize that the proposed scenarios for the Cs^+-rich and the Cs^+-lean mixture are mainly based on the ARXPS data probing only the first few nanometers. In future studies, these scenarios should be confirmed by complementary techniques such as surface X-ray scattering, which has not been done yet. Moreover, several details should be addressed in future investigations such as establishing a quantitative correlation between charging in XPS and solidification of ILs. Also is not well understood yet why the preferential formation of a solid $Cs[Tf_2N]$ surface layer around 100 °C was clearly observed for the Cs^+-rich 3 : 1 mixture while it was absent for the Cs^+-lean 1 : 3 mixture at temperatures around room temperature (and as expected from the phase diagram); possibly, nucleation theory might help in this context.

To conclude, we want to emphasize that surface depletion and enrichment effects as observed here for molten salt mixtures, can be of high practical relevance in applications where a large surface area is created to enhance the efficiency, *e.g.* in catalytic or separation processes with ionic media supported on highly porous solid supports.

Acknowledgements

R.G.B., P.S., B.S.J.H., F.M., and H.-P.S. thank the European Research Council (ERC) under the European Union's Horizon 2020 - Research and Innovation Programme for financial support, in the context of the Advanced Investigator Grant "ILID" to H.-P.S. (Grant Agreement No. 693398—ILID).

Appendix A. Supplementary data

Supplementary data to this article can be found online at https://doi.org/10.1016/j.molliq.2018.11.056.

References

[1] M.J. Earle, J.M.S.S. Esperanca, M.A. Gilea, J.N. Canongia Lopes, L.P.N. Rebelo, J.W. Magee, K.R. Seddon, J.A. Widegren, The distillation and volatility of ionic liquids, Nature 439 (2006) 831.
[2] N. Ito, R. Richert, Solvation dynamics and electric field relaxation in an imidazolium-PF_6 ionic liquid: from room temperature to the glass transition, J. Phys. Chem. B 111 (2007) 5016.
[3] P. Wasserscheid, Chemistry: volatile times for ionic liquids, Nature 439 (2006) 797.
[4] Ionic liquids in synthesis, in: P. Wasserscheid, T. Welton (Eds.), Ionic Liq. Synth., 2008, 2nd ed., vol. 1, Wiley-VCH Verlag GmbH & Co. KGaA, 2008.
[5] T. Welton, Ionic liquids in catalysis, Coord. Chem. Rev. 248 (2004) 2459.
[6] W. Xu, C.A. Angell, Solvent-free electrolytes with aqueous solution-like conductivities, Science 302 (2003) 422.
[7] F. Endres, S. Zein El Abedin, Air and water stable ionic liquids in physical chemistry, Phys. Chem. Chem. Phys. 8 (2006) 2101.
[8] E.F. Smith, F.J.M. Rutten, I.J. Villar-Garcia, D. Briggs, P. Licence, Ionic liquids in vacuo: analysis of liquid surfaces using ultra-high-vacuum techniques, Langmuir 22 (2006) 9386.
[9] M. Sobota, M. Schmid, M. Happel, M. Amende, F. Maier, H.-P. Steinrück, N. Paape, P. Wasserscheid, M. Laurin, J.M. Gottfried, J. Libuda, Ionic liquid based model catalysis: interaction of [BMIM][Tf_2N] with Pd nanoparticles supported on an ordered alumina film, Phys. Chem. Chem. Phys. 12 (2010), 10610.
[10] K.R.J. Lovelock, I.J. Villar-Garcia, F. Maier, H.-P. Steinrück, P. Licence, Photoelectron spectroscopy of ionic liquid-based interfaces, Chem. Rev. 110 (2010) 5158.
[11] H.-P. Steinrück, Recent developments in the study of ionic liquid interfaces using X-ray photoelectron spectroscopy and potential future directions, Phys. Chem. Chem. Phys. 14 (2012) 5010.
[12] O. Höfft, S. Bahr, M. Himmerlich, S. Krischok, J.A. Schaefer, V. Kempter, Electronic structure of the surface of the ionic liquid [EMIM][Tf_2N] studied by metastable impact electron spectroscopy (MIES), UPS, and XPS, Langmuir 22 (2006) 7120.
[13] A. Kauling, G. Ebeling, J. Morais, A. Padua, T. Grehl, H.H. Brongersma, J. Dupont, Surface composition/organization of ionic liquids with Au nanoparticles revealed by high-sensitivity low-energy ion scattering, Langmuir 29 (2013) 14301.
[14] I.J. Villar-Garcia, S. Fearn, G.F. De Gregorio, N.L. Ismail, F.J.V. Gschwend, A.J.S. McIntosh, K.R.J. Lovelock, The ionic liquid-vacuum outer atomic surface: a low-energy ion scattering study, Chem. Sci. 5 (2014) 4404.
[15] G. Law, P.R. Watson, A.J. Carmichael, K.R. Seddon, Molecular composition and orientation at the surface of room-temperature ionic liquids: effect of molecular structure, Phys. Chem. Chem. Phys. 3 (2001) 2879.
[16] A.B. Biedron, E.L. Garfunkel, E.W. Castner, S. Rangan, Ionic liquid ultrathin films at the surface of Cu(100) and Au(111), J. Chem. Phys. 146 (2017) (054704/1).
[17] R. Wen, B. Rahn, O.M. Magnussen, In situ video-STM study of adlayer structure and surface dynamics at the ionic liquid/Au (111) interface, J. Phys. Chem. C 120 (2016) 15765.
[18] F. Maier, I. Niedermaier, H.P. Steinrück, Perspective: chemical reactions in ionic liquids monitored through the gas (vacuum)/liquid interface, J. Chem. Phys. 146 (2017), 170901.
[19] E.J. Smoll, M.A. Tesa-Serrate, S.M. Purcell, L. D'Andrea, D.W. Bruce, J.M. Slattery, M.L. Costen, T.K. Minton, K.G. McKendrick, Determining the composition of the vacuum–liquid interface in ionic-liquid mixtures, Faraday Discuss. 206 (2018) 497.
[20] C. Van Doorslaer, J. Wahlen, P. Mertens, K. Binnemans, D. De Vos, Immobilization of molecular catalysts in supported ionic liquid phases, Dalton Trans. 39 (2010) 8377.
[21] H.P. Steinrück, J. Libuda, P. Wasserscheid, T. Cremer, C. Kolbeck, M. Laurin, F. Maier, M. Sobota, P.S. Schulz, M. Stark, Surface science and model catalysis with ionic liquid-modified materials, Adv. Mater. 23 (2011) 2571.
[22] M. Sobota, M. Happel, M. Amende, N. Paape, P. Wasserscheid, M. Laurin, J. Libuda, Ligand effects in SCILL model systems: site-specific interactions with Pt and Pd nanoparticles, Adv. Mater. 23 (2011) 2617.
[23] C. Maton, N. De Vos, C.V. Stevens, Ionic liquid thermal stabilities: decomposition mechanisms and analysis tools, Chem. Soc. Rev. 42 (2013) 5963.
[24] M. Scheuermeyer, M. Kusche, F. Agel, P. Schreiber, F. Maier, H.-P. Steinrück, J.H. Davis, F. Heym, A. Jess, P. Wasserscheid, Thermally stable bis(trifluoromethylsulfonyl)imide salts and their mixtures, New J. Chem. 40 (2016) 7157.
[25] I. Niedermaier, C. Kolbeck, H.P. Steinrück, F. Maier, Dual analyzer system for surface analysis dedicated for angle-resolved photoelectron spectroscopy at liquid surfaces and interfaces, Rev. Sci. Instrum. 87 (2016) 045105.
[26] S. Men, B.B. Hurisso, K.R.J. Lovelock, P. Licence, Does the influence of substituents impact upon the surface composition of pyrrolidinium-based ionic liquids? An angle resolved XPS study, Phys. Chem. Chem. Phys. 14 (2012) 5229.
[27] J.M. Gottfried, F. Maier, J. Rossa, D. Gerhard, P.S. Schulz, P. Wasserscheid, H.P. Steinrück, Surface studies on the ionic liquid 1-ethyl-3-methylimidazolium ethylsulfate using X-ray photoelectron spectroscopy (XPS), Z. Phys. Chem. 220 (2006) 1439.